Journal of Chromatography A, 1218 (2011) 1780–1789

Contents lists available at ScienceDirect

Journal of Chromatography A

journal homepage: www.elsevier.com/locate/chroma

# A continuous DC-insulator dielectrophoretic sorter of microparticles

Soumya Keshavamurthy Srivastava[a], Javier L. Baylon-Cardiel[b], Blanca H. Lapizco-Encinas[c], Adrienne Robyn Minerick[d,*]

[a] Voiland School of Chemical Engineering and Bioengineering, Washington State University, Pullman, WA, USA
[b] BioMEMS Research Chair, Tecnológico de Monterrey, Campus Monterrey, Monterrey, NL 64849, Mexico
[c] Centro de Investigación y de Estudios Avanzados del IPN Unidad Monterrey, Vía del Conocimiento 201, PIIT, Apodaca, NL 66600, Mexico
[d] Department of Chemical Engineering, Michigan Technological University, 1400 Townsend Drive, Houghton, MI, USA

ARTICLE INFO

*Article history:*
Received 8 October 2010
Received in revised form 21 January 2011
Accepted 27 January 2011
Available online 4 February 2011

*Keywords:*
Dielectrophoresis
Microfluidics
Polystyrene particles
Insulator dielectrophoresis

ABSTRACT

A lab-on-a-chip device is described for continuous sorting of fluorescent polystyrene microparticles utilizing direct current insulating dielectrophoresis (DC-iDEP) at lower voltages than previously reported. Particles were sorted by combining electrokinetics and dielectrophoresis in a 250 μm wide PDMS microchannel containing a rectangular insulating obstacle and four outlet channels. The DC-iDEP particle flow behaviors were investigated with 3.18, 6.20 and 10 μm fluorescent polystyrene particles which experience negative DEP forces depending on particle size, DC electric field magnitude and medium conductivity. Due to negative DEP effects, particles are deflected into different outlet streams as they pass the region of high electric field density around the obstacle. Particles suspended in dextrose added phosphate buffer saline (PBS) at conductivities ranging from 0.50 to 8.50 mS/cm at pH 7.0 were compared at 6.85 and 17.1 V/cm. Simulations of electrokinetic and dielectrophoretic forces were conducted with *COMSOL Multiphysics*® to predict particle pathlines. Experimental and simulation results show the effect of medium and voltage operating conditions on particle sorting. Further, smaller particles experience smaller iDEP forces and are more susceptible to competing nonlinear electrostatic effects, whereas larger particles experience greater iDEP forces and prefer channels 1 and 2. This work demonstrates that 6.20 and 10 μm particles can be independently sorted into specific outlet streams by tuning medium conductivity even at low operating voltages. This work is an essential step forward in employing DC-iDEP for multiparticle sorting in a continuous flow, multiple outlet lab-on-a-chip device.

© 2011 Elsevier B.V. All rights reserved.

## 1. Introduction

Lab-on-a-chip (LOC) systems have the capacity to perform a variety of tasks ranging from DNA analysis to protein recognition and could be catered to point-of-care medical diagnostic tools. They integrate multiple laboratory functions on a few centimeter(s) sized chip and are capable of handling picoliter fluid volumes [1–4]. Electrokinetics is commonly employed to move analytes in microdevices since electric fields are versatile and can be precisely controlled for specific, quantifiable analyte responses. Furthermore, devices employing electric fields can eventually be simplified to only require a battery for power – a key characteristic for truly portable diagnostic devices. One type of electrokinetic phenomenon, dielectrophoresis (DEP), has traditionally employed alternating current (AC) electric fields to create spatial nonuniformities which impart forces on particles or cells through transient polarizations. Dielectrophoresis can also be achieved using direct current (DC) electric fields and this paper focuses on employing DC electric fields to achieve continuous sorting of fluorescent polystyrene particles.

Direct current insulating dielectrophoresis (DC-iDEP) is a relatively new field that has yielded >50 journal publications over the last decade [5]. It utilizes a spatially non-uniform electric field component but not the frequency dependent component of AC-dielectrophoresis, which has been shown to be adequate for manipulation of cells [4,5]. Spatial non-uniformities in the electric field are generated via insulating obstacles embedded within the microdevice channels, while remotely positioned electrodes at the ends of the channels deliver either (a) direct current (DC-iDEP) or (b) DC biased low frequency alternating current (AC-iDEP). The advantages of using such insulating obstacles to create nonuniformities in the channel include [6]: (a) less affected by fouling than embedded electrodes, (b) fabrication is simpler because no embedded metal components are required, (c) devices are robust and chemically inert, (d) electrolysis gas evolution at the remotely located metal electrodes causes minimal or no bubbles inside channels, and (e) microdevices are continuous flow systems and can be operated with complex electrical signals.

* Corresponding author. Tel.: +1 906 487 2796; fax: +1 906 487 3213.
*E-mail address:* minerick@mtu.edu (A.R. Minerick).

0021-9673/$ – see front matter © 2011 Elsevier B.V. All rights reserved.
doi:10.1016/j.chroma.2011.01.082

Pioneering work on DC-iDEP contained an array of insulating posts where two operating regimes were observed, namely streaming and trapping DEP [7]. In streaming DEP, particles of interest experience repulsion from electric field maxima but travel through the device in flowing streamlines; and in trapping DEP the forces reversibly immobilize the particles of interest. Performance characterization of a DC-iDEP microdevice assessed the effects of suspending medium properties on dielectrophoretic trapping. Results indicate that higher conductivity medium increased trapping efficiency [8]. To the authors' knowledge, optimization of particle streaming efficiencies has not been conducted. Studies on DC-iDEP mainly rely on negative dielectrophoresis (nDEP) since under DC or low-frequency AC electric fields inert particles, macromolecules and cells are less conductive than the suspending medium.

Microdevice fabrication has been achieved with different materials which influence wall surface charge and thus electro-osmotic velocities, but all achieve field non-uniformities governed by obstacle geometries. There have been many efforts to explore other insulating materials for DC-iDEP including oil droplets [9] and pairs of insulating oil menisci to shape the DC electric field [10]. Other researchers have explored differently shaped insulating obstacles like rectangle [11], triangle [11], circular [12], saw-tooth [13,14], serpentine channels [15,16], circular posts [17,18] and open top microstructures [19,20]. Researchers have also explored using DC biased AC fields for achieving specialized separations of particles and cells [16,21–24]. A complete picture of particle shape, insulating obstacle geometry and voltage dependencies of direct current insulator-based dielectrophoresis has not yet been attained. The DC voltages reported in the literature to achieve sorting of microparticles were in the high range of 250–5000 V/cm and this may increase Joule heating in microdevices. A range of operating variables with respect to medium characteristics, field characteristics, particle sizes and characteristics, and insulating obstacle geometry still remains ill defined.

In the present research, rectangular PDMS insulating obstacles were utilized to create a spatially non-uniform electric field to sort three different sized particles (3.18 μm, 6.20 μm and 10 μm) into four channel outlets using only DC electric fields. The DC field's interactions with the wall surface charges simultaneously pump liquid via electro-osmotic flow (EOF), thus eliminating micropumps and increasing portability. This research aims to provide a working range of electric field and medium conductivities for polystyrene particle sorting in a continuous flow device. In order to prevent Joule heating and salt formation at electrodes, low medium conductivities and low electric fields were utilized.

## 2. Theoretical background

### 2.1. Particle motion

Particle transport along the microchannel was assumed to depend on electrokinetic (EK) and dielectrophoretic (DEP) mechanisms only. The particle flux $\vec{j}$ is expressed in terms of an electrokinetic velocity $\vec{u}_{EK}$ and dielectrophoretic $\vec{u}_{DEP}$ velocities as

$$\vec{j} \propto (\vec{u}_{EK} + \vec{u}_{DEP}) \tag{1}$$

The electrokinetic velocity, $\vec{u}_{EK}$ takes into account the electrophoretic and electro-osmotic contributions to the particle transport. The apparent velocity is taken to be proportional to the applied electric field $\vec{E}$, as

$$\vec{u}_{EK} = \mu_{EK}\vec{E} = (\mu_{EP} + \mu_{EO})\vec{E} \tag{2}$$

where $\mu_{EK}$, $\mu_{EP}$, $\mu_{EO}$ are the electrokinetic, electrophoretic, and electro-osmotic mobilities, respectively. For relatively large particle size with low surface charge it is possible to neglect the electrophoretic mobility [8], thus:

$$\mu_{EK} \approx \mu_{EO} \tag{3}$$

$$\mu_{EO} = \frac{\zeta\varepsilon_m}{\eta} \tag{4}$$

where $\zeta$, $\varepsilon_m$, $\eta$ are zeta potential of the microchannel wall, permittivity of suspending medium and viscosity of suspending medium, respectively.

The dielectrophoretic velocity $\vec{u}_{DEP}$ is related to the applied electric field as

$$\vec{u}_{DEP} = -\mu_{DEP}\nabla E^2 \tag{5}$$

where $\mu_{DEP}$ is the dielectrophoretic mobility. For a spherical particle of diameter $d_p$, the dielectrophoretic mobility $\mu_{DEP}$ can be is expressed as [1]:

$$\mu_{DEP} = \frac{\pi {d_p}^2 f_{CM}\varepsilon_m}{12\eta} \tag{6}$$

where $f_{CM}$ is the Clausius–Mossotti factor, which accounts for the particle polarizability. Under a DC electric field, for a spherical particle with a conductivity $\sigma_p$ suspended in a medium with conductivity $\sigma_m$ the $f_{CM}$ is given by [25]:

$$f_{CM} = \frac{\sigma_p - \sigma_m}{\sigma_p + 2\sigma_m} \tag{7}$$

As it can be observed from Eq. (7), $f_{CM}$, DEP can be positive or negative, depending on the relative conductivities of the particle and suspending medium. It has been shown that for a DC electric field, polystyrene particles [8,26] and bacterial cells [14,27] exhibit negative dielectrophoresis: *i.e.*, they are less conductive than the suspending medium and are repelled from the regions of higher field density. In this research, the microdevice developed exploits these characteristics in order to sort the particles into four outlet channels via a unique device design. In this study, conductivity of the polystyrene particle was considered negligible ($\sigma_p$ = 0 mS/cm) compared to that of the suspending medium [26]. This assumption was supported by $\sigma_p$ values reported in the literature [26] where all values for $f_{CM}$ were close to −0.5.

A spatially dense non-uniform field is created around the obstacle as the DC field lines diverge around the insulating obstacle. Due to the presence of the insulating obstacle, a high electric field density region is produced between the obstacle and the channel wall, which imparts a DEP force on particles flowing down the channel thus altering their trajectory into one of the four outlet channels. These negative DC-iDEP forces push the particles away from high field density regions resulting in a repulsive force exerted on the particle as it flows around the corner of the obstacle, thus facilitating particle motion. From Eq. (7), since $\sigma_p < \sigma_m$ the particles experience repulsive forces yielding streaming DEP.

### 2.2. Particle pathlines

In experiments, the fluorescent particles moved rapidly to cause streaks in each still frame image. Therefore, particle pathlines were used in the simulations to represent particle motion. Particle pathlines are the trajectories that individual particles follow when experiencing electrokinetic and dielectrophoretic forces. The direction the particle takes is also influenced by fluid streamlines at each moment of time. Since the polystyrene particles had similar dielectric properties and thus $f_{CM}$, the effect of DEP on a particle pathline depended primarily on particle diameter (Eq. (6)). The magnitude of the DEP force depends on $E^2$, which reaches its maximum in the region where the insulating obstacle is located. At a given medium conductivity, particles which come out of the constriction region

**Table 1**
Average conductivities of various dextrose added buffers with standard deviations and electro-osmotic mobility with standard deviations for each buffer at 10.3 V/cm. The number *n* represents the number of solutions averaged for calculating buffer conductivities. The values ranged between 0.50 and 8.50 mS/cm and do not show a mobility dependence on buffer conductivity.

| % dextrose added buffers | Average conductivity (mS/cm) | Electroosmotic mobility ($\times 10^{-4}$ cm$^2$/V s) |
|---|---|---|
| 5% | 0.24 ± 0.009 ($n$ = 5) | 41.9 ± 2.40 |
| 4% | 5.58 ± 0.028 ($n$ = 4) | 36.9 ± 0.96 |
| 3% | 6.16 ± 0.041 ($n$ = 5) | 41.0 ± 1.53 |
| 2% | 7.32 ± 0.035 ($n$ = 4) | 53.5 ± 5.05 |
| 1% | 8.23 ± 0.032 ($n$ = 4) | 54.2 ± 1.92 |
| 0% (PBS) | 8.47 ± 0.024 ($n$ = 2) | 32.9 ± 1.07 |

will be deflected due to the differing nDEP force to different channel outlets, depending on their diameter.

### 2.3. Mathematical model

The iDEP microdevice performance was studied with a mathematical model built in *COMSOL Multiphysics*® implementing Finite Element Analysis (FEA). AutoCAD drawings of the device were imported into COMSOL. By solving the Laplace equation, predictions were made on the distribution of electric potential across the microdevice, the magnitude of the electrokinetic forces involved, and the particle trajectories. For the model, the applied DC electric potential was assumed to remain constant throughout the microchannel depth; it has been demonstrated that the electric field does not decay in a significant manner along the depth [25]. Therefore, the simulation was treated as a two-dimensional electrostatics problem.

A triangular mesh was built in order to solve the Laplace equation using the *Lagrange element* implemented in the software. FEA was applied in a triangular mesh consisting of 1200 elements and 2800 nodal points. The electric potential was approximated by a polynomial of low order at each mesh point. From the obtained numerical solution it is possible to obtain values for the parameters describing the electrokinetic and dielectrophoretic behavior of the particles, such as the electrical field $\vec{E}$, gradient of $E^2$, and particle pathlines. Values for the electrokinetic mobility were obtained from reported experimental results (shown in Table 1); this is described in the experimental methods section under sample preparation.

The microchannel contained one embedded rectangular insulating obstacle and four different outlet channels (Fig. 1). When applying a DC electric potential, the presence of the insulating obstacle creates a region of non-uniform electric field that affects particle pathlines by means of negative dielectrophoretic effects. Further information regarding microchannel geometry is included in the Experimental Methods section under device design. The model solves the electrical potential inside the microchannel as described by the Laplace equation:

$$\nabla^2 \phi = 0 \tag{8}$$

with boundary conditions:

$$\vec{n} \cdot \vec{J} = 0 \quad \text{at the boundaries} \tag{9}$$

$$\phi = \phi_{in} \quad \text{at the inlet of the microchannel} \tag{10}$$

$$\phi = 0 \quad \text{at the outlet of the microchannel} \tag{11}$$

From the numerical solution obtained, it is possible to predict the motion of the spherical particles along the microchannel [28].

## 3. Experimental methods

From Eqs. (5)–(7), dielectrophoretic force on the particle depends on magnitude of the applied DC electric field, medium conductivity, and size of fluorescent polystyrene particles. All these dependencies were explored. In this section device design and microdevice fabrication, experimentation for electro-osmotic flow assessment and fluorescent polystyrene particle experiments, image analysis and quantification are discussed in detail.

### 3.1. Device design and fabrication

The microdevice developed consists of one inlet (250 μm wide) and four outlet channels of 90 μm in width. The purpose of this design containing four branched outlets was to incorporate multi-particle sorting. The distance between the inlet and outlet ports was 1.46 cm with 3 mm diameter ports. An insulating obstacle of rectangular geometry was positioned in the inlet channel at a distance of 150 μm upstream from the bifurcation to the four outlet channels. The width of the rectangular obstacle was 330 μm and the height was 190 μm as shown in Fig. 1. Standard techniques of soft lithography were used to pattern the microdevice and microchannels [29] that were cast into poly(dimethylsiloxane) (PDMS) device and sealed onto a glass slide by plasma-oxidation treatment (Harrick Plasma, Inc.) [30,31]. A single platinum (Pt) electrode was woven through the outlet ports.

### 3.2. Sample preparation

For reduced Joule heating and to increase streaming DEP on the particles, low conductivity buffers were desired. A range of medium conductivities were explored in this research and separation efficiency of polystyrene particles was studied. Phosphate buffer saline (PBS) with dextrose was used to obtain a range of medium conductivities. D-Glucose (dextrose) (Fisher Scientific, >99% pure, anhydrous) was added to PBS at concentrations ranging from 1 to 5 wt%; pH was adjusted to 7.0 for the solutions using HCl and NaOH (Fisher Scientific, HPLC grade) as necessary and final conductivities were recorded for each buffer. Table 1 indicates the average conductivity values with standard deviations obtained for all the dextrose-added buffers over the range of solutions prepared ($n$). The conductivities varied between 0.50 and 8.50 mS/cm. Here 0% buffer refers to 0.14 M PBS (1×) at pH 7.0.

### 3.3. Operation

As demonstrated in Eq. (6), the dielectrophoretic mobility that a particle experiences is proportional to its volume (and subsequently its size) as well as the conductivity difference ($f_{CM}$) from the surrounding medium [27]. Therefore, dependencies on fluorescent polystyrene particles of three sizes were studied here as well as on six different conductive buffers. The details of electro-osmotic mobility measurement experiments and polystyrene particle experiments are presented in the next two sections.

#### 3.3.1. Electro-osmotic flow measurement

Electro-osmotic flow rate experiments within the main channel into the four outlet channels were conducted by current monitoring methods [32]. The set-up consists of 1 kΩ–1/2 kW resistor, multimeter (0–500 V) (RadioShack, Inc.), and a DC power supply (Hewlett Packard 6030A, 0–200 V, 17 A). Electrical connections with PDMS microdevice were made by using copper electrodes. The experiment was conducted at 10.3 V/cm for plasma-sealed devices using 0.56 M PBS buffer and dextrose added buffers at varying conductivity ranges (0.50–8.50 mS/cm) as shown in Table 1. The impact on EOF from alternative sealing mechanisms were also explored

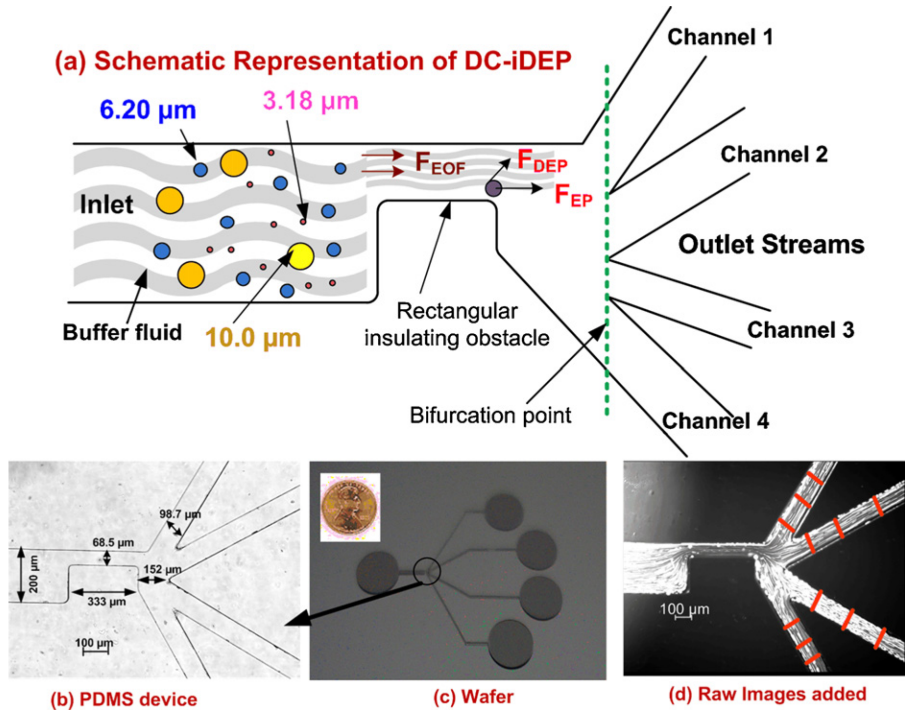


**Fig. 1.** (a) A particle at the insulating obstacle due to electric field $\vec{E}$, experiences electrophoretic force '$F_{EP}$' (negligible in this research due to particle size), electro-osmotic force '$F_{EO}$' from the fluid, and the dielectrophoretic force '$F_{DEP}$'. (b) Rectangular obstacle geometry enlarged from (c) at the point highlighted bifurcating into four channels. (c) Master on silicon wafer showing device design of 1.46 cm in length compared to the size of a penny. (d) Raw images from 3.18 µm particle experiments added by Maximum Intensity Projection (MIP) in AxioVision 4.6.3 software. Intensity profiles (shown in red lines) are drawn across each outlet channel at three different positions. Particles quantified by comparing relative profile intensity across each channel. (For interpretation of the references to color in the figure caption, the reader is referred to the web version of the article.)

including common methods like UV–ozone sealed [33] solvent method using IPA [34], thermal treatment [35] and no treatment for PDMS and glass-slide sealed by pressure application.

The microchannels were pre-conditioned by rinsing with e-pure water, and then filled with lower conductivity buffer (0.50–8.50 mS/cm) individually for each experimental set. DC power supply was turned on and initial voltage on multimeter was recorded when low conductivity buffer was present in the microdevice. The high conductivity buffer (4× PBS) replaced lower conductivity buffer (0.50–8.50 mS/cm dextrose added buffers) and the time required to reach a new constant voltage plateau across the resistor was measured. The experiment was repeated (standard deviation values in Table 1) at each DC electric field strength and statistical analysis performed on the measured times to replace the fluidic path with high conductivity buffer.

Particle movement depends on dielectrophoretic and electrokinetic mobility as shown in Eq. (1). To calculate dielectrophoretic mobility, electrokinetic mobility needs to be known. Electrokinetic mobility refers to EOF in this research (EP neglected as shown in Eq. (3)), and EOF causes particle movement towards the outlet direction whereas DEP deflects the particles into different channels. The electrokinetic mobility of buffers shown in Table 1 was calculated by the current monitoring technique [32] at 10.3 V/cm for all the medium conductivities. The time required to reach a voltage plateau when the buffers are replaced are noted and thus the electrokinetic mobilities (in this research, EK mobility is $\mu_{EO}$) for various buffers are calculated by:

$$\mu_{EK} = \mu_{EO} = \frac{L}{t\vec{E}} \tag{12}$$

where $L$, $t$, and $\vec{E}$, are the length of microdevice, time taken to reach the voltage plateau when one buffer replaces the other in the microchannel and applied DC electric field, respectively. It is important to note that in this system the $\mu_{EO}$ does not vary greatly and do not demonstrate a dependence on the conductivity of the buffer as shown in Table 1. These $\mu_{EO}$ values calculated from the current monitoring experiments using Eq. (12) at 10.3 V/cm were directly applied in all the simulations to predict particle pathlines.

### 3.3.2. Polystyrene particle experiments

Fluorescent polystyrene particles (Spherotech, Inc., Lake Forest, IL) of three different average diameters 3.18 µm (fluorescent pink, 580 nm emission), 6.20 µm (fluorescent ocean blue, 700 nm emission) and 10 µm (fluorescent yellow, 480 nm emission) were selected. Particle sizes were determined by the company using a NICOMP Laser Particle Sizer or visually by Scanning Electron Microscope. The co-efficient of variation for the three sizes were ∼12% indicating a narrow size distribution. So, polydispersity effects with regards to microparticle size, shape, and mass were assumed negligible and not controlled further in this study. Fluorescent polystyrene particles were diluted at 1:100 for 3.18 µm particles, 1:200 for 6.20 µm particles and 1:50 for 10 µm particles with all six buffers shown in Table 1. The dielectrophoretic mobilities, $\mu_{DEP}$ for the different sized particles were calculated from Eq. (6): 3.18 µm: $2.98 \times 10^{-11}$ cm$^4$/V s; 6.20 µm: $1.13 \times 10^{-10}$ cm$^4$/V s; 10 µm: $2.95 \times 10^{-10}$ cm$^4$/V s.

A DC power supply was used to deliver 10 or 25 V for separation of the particles over a distance of 1.46 cm between the inlet and outlet ports (corresponding to fields of 6.85 and 17.1 V/cm). The channels were filled with buffer initially and then 30 µL of buffer was replaced with the particle sample in the inlet port after the DC power supply was turned on. Experiments were repeated at least three times and statistical analysis performed on the results.

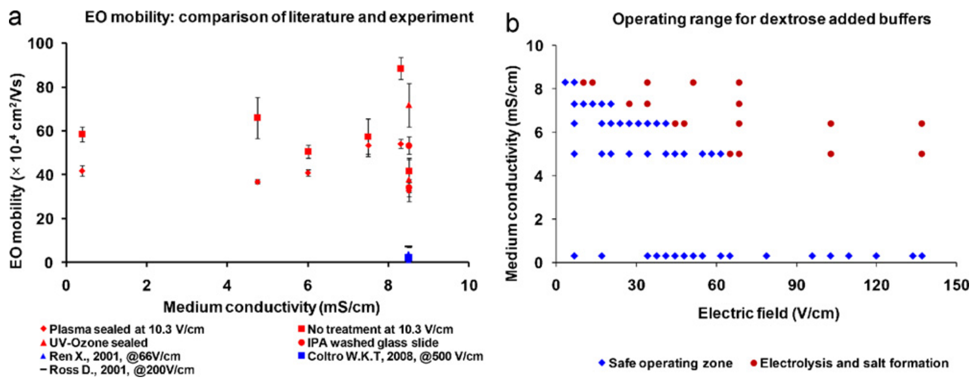


**Fig. 2.** (a) Electro-osmotic mobility of plasma-oxidation (in bold numbers), UV–ozone, IPA washed glass slide and no treatment (native PDMS channels) sealing methods. Comparison of literature reported values from Ren [36], Ross [40] and Coltro [39] groups are included for plasma sealed and native PDMS channels for PBS buffer. Average EOF value for plasma sealed device was $(40 \pm 2.32) \times 10^{-4}\,cm^2/V\,s$ at 10.3 V/cm. (b) Operating window for size dependency experiments at different buffer conductivity (0.50–8.50 mS/cm) and electric field strength (6.85–136 V/cm). Blue area is the safe operating zone for experiments, whereas in the red area heavy salt precipitation occurred at the inlet thus blocking the channels. (For interpretation of the references to color in the figure caption, the reader is referred to the web version of the article.)

Raw images of different sized fluorescent particles were taken with a CCD camera (Carl Zeiss, AxioCam MRm, 14 fps) attached to a pseudo-confocal microscope for 5 min at 0.25 s interval for each of the buffer conditions (0.50–8.50 mS/cm) and at DC field strengths of 6.85 and 17.1 V/cm.

#### 3.3.3. Image analysis

Two different analysis techniques were employed as a method of verifying the results obtained. (1) Quantification of particles in each channel was accomplished by using the Maximum Intensity Projection (MIP) program in Zeiss AxioVision software (version 4.6.3) by combining all raw images taken at every 0.25 s for 5 min. (2) For 6.20 and 10 μm particles, analysis was also verified by optically counting the particles in each channel for every 0.25 s un-altered video frames. An example of the composite image is shown in Fig. 1(d).

An intensity profile was drawn across each channel at three different positions. Care was taken to draw profile excluding (a) walls of the channel, (b) particles trapped at any points of field singularity and (c) particles settled in the channel. The particles were quantified by using Eq. (13), where $N_{Avg}^{Ch}$ is the number of particles present in each channel (Ch) averaged over three different positions ($X = 1, 2, 3$); $I_{Total}^{Ch}$ is the total intensity of all the particles in a channel at one position $X$; $I_{p,Avg}$ is the average intensity of one particle. Total particle fraction in each channel was calculated by Eq. (14), where $F^{Ch}$ denotes the fraction of particles present in one outlet channel ($Ch = 1, \ldots, 4$). Thus particle fractions for all the three sizes of particles at different buffer conditions were calculated by indirect quantification via the relative intensity profile method.

$$N_{Avg}^{Ch} = \frac{Avg\left[\sum_{X=1}^{3} I_{Total}^{Ch}\right]}{I_{p,avg}} \tag{13}$$

$$F^{Ch} = \frac{N_{Avg}^{Ch}}{\sum_{Ch=1}^{4} N_{Avg}^{Ch}} \tag{14}$$

$$F^{Ch} = \frac{P_T^{Ch}}{\sum_{Ch=1}^{4} P_T^{Ch}} \tag{15}$$

In the direct quantification approach to image analysis, particles in each channel were optically counted and fractions were calculated by using Eq. (15), where $F^{Ch}$ denotes the fraction of particles present in one outlet channel ($Ch = 1, \ldots, 4$). This method of quantification was only used for large sized particle (6.20 and 10 μm), as individual particles were optically more distinguishable than 3.18 μm particles.

## 4. Results and discussions

### 4.1. Electro-osmotic flow measurement and baseline study

Theory predicts that particle motion depends on electro-osmotic and dielectrophoretic mobilities. Under microparticle streaming DEP conditions, dielectrophoretic forces are comparable to EOF. Lower applied potentials are preferred to avoid Joule heating, electrolysis, and related contributions and will simultaneously increase relative dielectrophoretic effects by reducing EOF. To reduce EOF in the designed microdevice, different sealing techniques and surface channel coatings were explored. Comparisons were made between literature reported values and experimental values for native PDMS channels and PDMS channels sealed by plasma oxidation [36–40] for PBS buffer at ~8.50 mS/cm and pH 7.0 (Fig. 2(a)). A UV–ozone sealing treatment increased the $\mu_{EO}$ while channels coated with Tween 20 [41] (99.9%, Fisher Scientific) and 5% 8000 MW polyvinyl propylene (PVP) reduced $\mu_{EO}$ by 10%. Plasma-oxidation sealing minimized EOF and was adopted for all subsequent experiments. The average $\mu_{EO}$ at 10.3 V/cm was $(40 \pm 2.32) \times 10^{-4}\,cm^2/Vs$ although $\mu_{EO}$ showed slight variations with buffer conductivities. This change in $\mu_{EO}$ influences the length of time a particle flowing through the system experiences a DEP force as it passes by the insulating obstacle.

An optimal operating window for the microdevice was determined as shown in Fig. 2(b). Two different behavior regions were observed for six buffers in electric fields from 6.85 to 136 V/cm. At lower conductivities (0.50 mS/cm), no noticeable electrolysis was observed, but at higher conductivities (4.75–8.50 mS/cm) the maximum permissible voltage without any detectable electrolysis was sequentially reduced. The blue diamonds in Fig. 2(b) indicate the safe operating regions; red circles identify adverse operating conditions due to electrolysis and precipitant formation at electrodes.

### 4.2. Size dependency

Experiments with fluorescent polystyrene particles of three different sizes were conducted to observe size-dependent particle trajectory patterns near the insulating obstacle region and into the four outlet channels. Particles experienced complex non-linear nDEP forces resulting in unique distributions of particles.

#### 4.2.1. 3.18 μm particles

Due to the smaller particle size and their high velocity in the DC-iDEP channel system, 3.18 μm particle flow events were quantified in each of the four channels with MIP. Intensity as a function

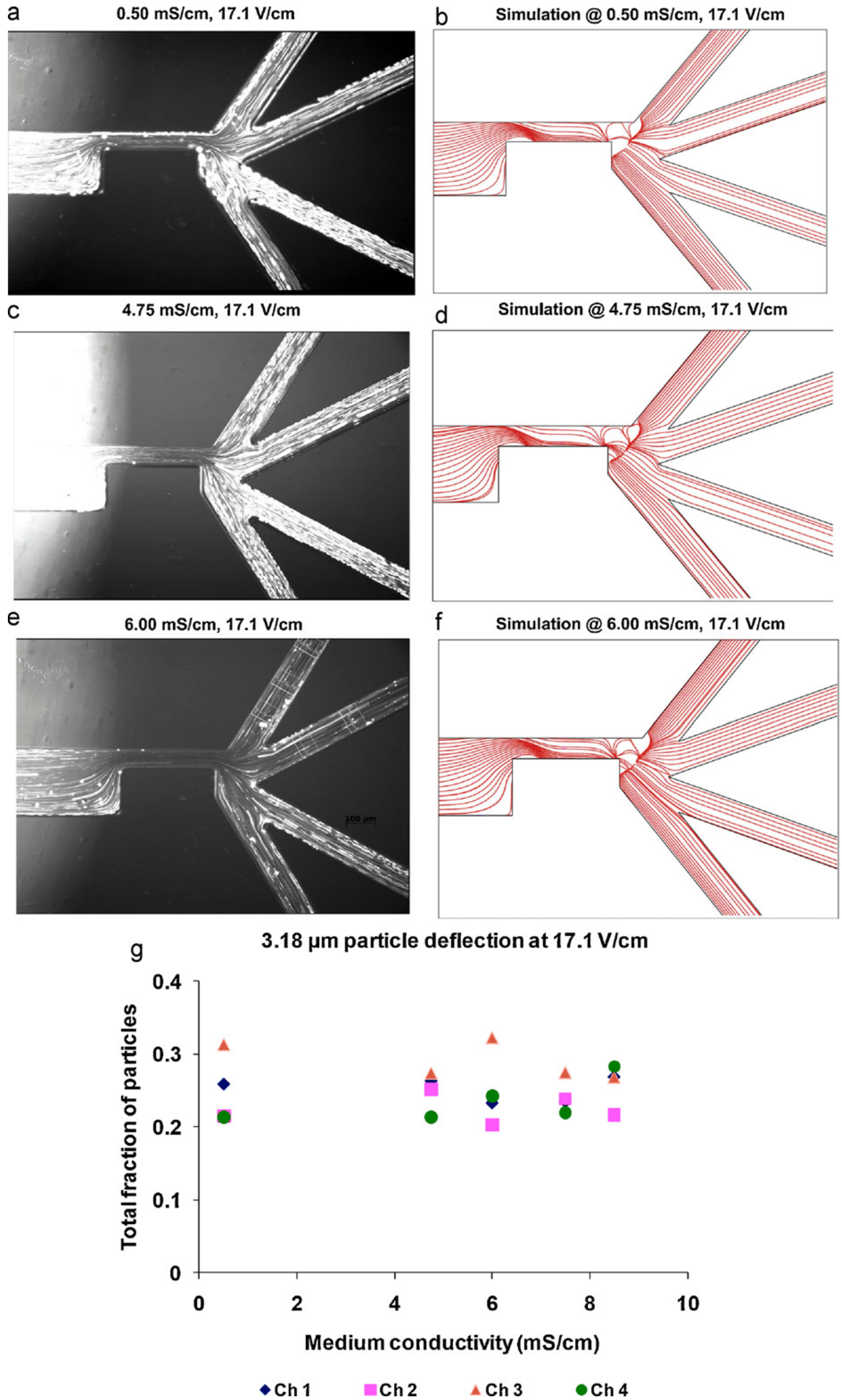


**Fig. 3.** (a, c and e) Raw images of 3.18 μm particle trajectories overlaid by MIP program at 0.50, 4.75 and 6.00 mS/cm and 17.1 V/cm. (b), (d) and (f) simulations of particle trajectories obtained for 3.18 μm particles at 17.1 V/cm, 0.50, 4.75 and 6.00 mS/cm. Channels 3 and 4 are preferred at 17.1 V/cm. (g) Deflection of 3.18 μm particles at 17.1 V/cm over a range of buffer conductivities. The particles could be directed towards channel 3 using a particular combination of electric field and medium conductivity.

of position was generated for each image in the time sequence and intensity spikes were observed for each particle flowing event. At different conductivities, the particle concentrations varied in each channel as shown in Fig. 3(g). From Fig. 3(a), (c), (e) and (g)) channel 3 had slightly higher particle fractions at most medium conductivities, but in general 3.18 μm particles were relatively uniformly distributed across all four channels suggesting that any DEP effects were minimal.

Simulations were conducted to predict the electrokinetic trajectories of the 3.18 μm particles at 0.50, 4.75 and 6.00 mS/cm at an electric field of 17.1 V/cm utilizing electrokinetic mobility values (Table 1) calculated from Eq. (12). Fig. 3(b), (d) and (f) shows

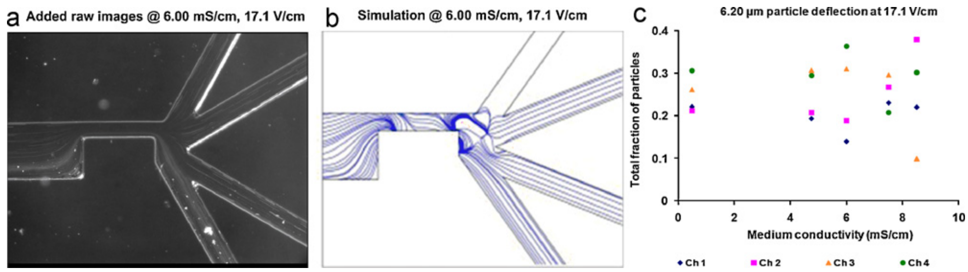


**Fig. 4.** (a) Raw images of 6.20 μm particle trajectories combined by MIP program at 6.00 mS/cm and 17.1 V/cm. (b) Simulations of particle trajectories obtained for 6.20 μm particles at 17.1 V/cm and 6.00 mS/cm. Particles deflected into channel 4 at 17.1 V/cm and lower conductivities. (c) Deflection of 6.20 μm particles at 17.1 V/cm over a range of buffer conductivities.

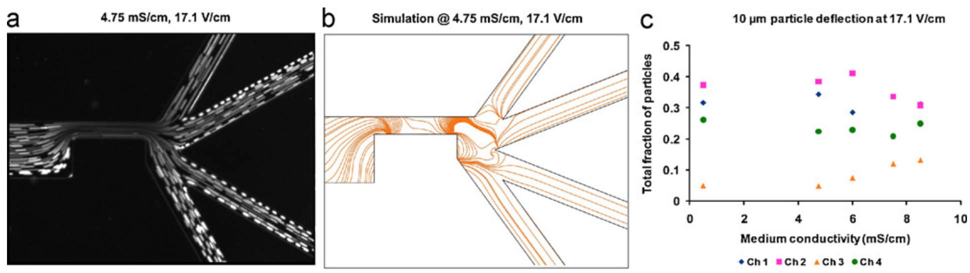


**Fig. 5.** (a) Raw images of 10 μm particle trajectories combined by MIP program at 4.75 mS/cm, 17.1 V/cm. (b) Simulated particle trajectories obtained for 10 μm particles at 17.1 V/cm, 4.75 mS/cm. Most particles were deflected towards channel 2. (c) Deflection of 10 μm particles at 17.1 V/cm over a range of buffer conductivities. Experimental observations indicate that most particles experienced less deflection compared to 6.20 μm particles.

the predicted pathlines of particles. By comparing these results with the experimental results, weak qualitative agreement exists that DEP effects are minimal such that no strong channel preference exists. Further, the simulations show unusual particle trapping events indicated by pathlines ending at channel or obstacle surfaces as well as pathlines converging to a single point between the trailing edge of the obstacle and the channel bifurcation. Such behaviors were not observed in the experiments as shown in Fig. 3(a), (c), and (e). Recirculations around the obstacle are caused when the dielectrophoretic force (non-linear) component dominates electrokinetic (linear) force component. This is observed in regions where the electric field gradient is large due to sharp angle singularities in the geometry. Within the physically realized microdevice, these angles are rounded, field leakage through the corners of walls is possible, and small electrophoretic and hydrodynamic effects likely smooth out the particle pathlines.

*4.2.2. 6.20 μm particles*

The flow patterns of 6.20 μm particles were also quantified using the raw images by MIP. This resulted in composite images showing particle streaks down the length of outlet channels (Fig. 4(a)). Experiments were run at 17.1 V/cm and five different buffer conductivities. Using Eqs. (13) and (14), the total number of particles, and fractions for each channel and for each electric field condition were obtained. Experimental results suggested that the channel preference for 6.20 μm particles was channel 4 for low buffer conductivities as shown in Fig. 4(c). Direct quantification of particle events using Eq. (15) was also conducted. The particle fractions obtained by this method were in close agreement with the indirect quantification method. Simulations shown in Fig. 4(b) were conducted to predict the electrokinetic trajectories of the 6.20 μm particles employing 6.00 mS/cm buffer conductivity and 17.1 V/cm. Again, a rough qualitative agreement exists with the experimental results in which a majority of particle pathlines enter outlet channel 4 (∼37% experimentally), reducing fractions in channels 3 and 2 and minor particle events in channel 1 (∼13% experimentally). Simulations again show recirculations and trapping events which are not observed in experiments. Fig. 4(c) does not demonstrate a clear trend of channel preference with changing conductivity, which again supports that DEP forces and EOF behaviors, both of which are functions of medium conductivity, do not fully describe the particle motion observed in these experiments.

*4.2.3. 10 μm particles*

A composite MIP image for 10 μm particles is shown in Fig. 5(a) for 4.75 mS/cm and 17.1 V/cm conditions. These large particles were slowed along the channel walls due to particle wall electrostatic interactions. In the composite MIP image, slower moving particles yield more intense streaks. The particle events in each channel were compiled in Fig. 5(c); channels 1 and 2 each captured a third or greater of the total particles at 17.1 V/cm. To verify the experimental results obtained by intensity profile analysis, direct quantification was also conducted using Eq. (15) and was in close agreement with the indirect quantification method. In Fig. 5(b), 10 μm simulated particle pathlines at 4.75 mS/cm, 17.1 V/cm are shown which indicate more severe pathline terminations at surfaces and recirculations. The reliability of the simulated predictions appears to decrease with increasing particle size likely due to the greater calculated DEP force which is a combination of the field gradient singularity effects and the larger particle radius terms as illustrated in Eq. (6).

From size dependency studies, it is possible to observe that the electro-osmotic forces on 3.18 μm particles nearly equal the DEP forces such that these smaller particles are nearly uniformly distributed across the four outlet channels. 6.20 μm particles experience weak, but measurable DEP forces over the linear electrokinetic forces and are directed around the obstacle into channels 4 and 3 with very few events in channel 1. Lastly, 10 μm particles experienced the greatest nDEP forces with deflection from the insulating obstacle into channels 2 and 1. Since $\mu_{DEP}$ is proportional to the square of the particle diameter, larger DEP forces for larger particles was roughly verified in a complex four-channel device.

*4.3. Electric field dependency*

The dielectrophoretic force that acts normal to the insulating obstacle surface is proportional to $E^2$ (Eq. (5)). To explore this phenomenon, experiments were conducted for 6.20 μm particles at

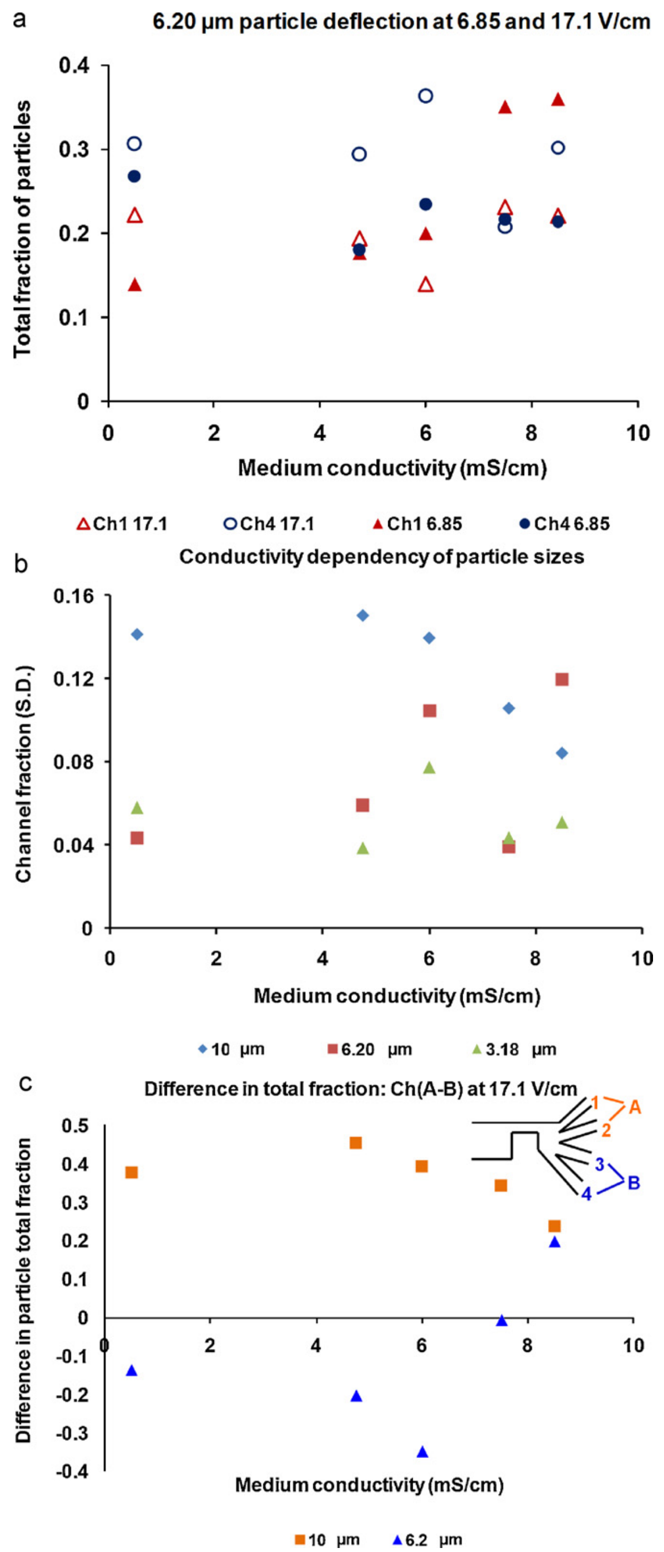


**Fig. 6.** (a) Experimental channel particle fractions for 6.20 µm particles at electric field conditions of 6.85 and 17.1 V/cm plotted as a function of medium conductivity for channels 1 and 4. Higher electric fields (17.1 V/cm) and low medium conductivities (<6 mS/cm) yield better separations, (b) channel fraction SD for 3.18 µm (green triangles), 6.20 µm (red squares) and 10 µm (blue diamond) particles at electric field conditions of 17.1 V/cm plotted as a function of medium conductivity. High particle fractions and better sorting is achieved at 6 mS/cm for all particle sizes, (c) deflection of 6.20 µm (blue triangles) and 10 µm (orange squares) particles in a mapped 2-channel system at different medium conductivity values. Inset shows the 2-channel system where channel A is the sum of channels 1 and 2; channel B is the sum of channels 3 and 4. Positive particle fraction difference 'δ' indicates particles are deflected into channel A and negative indicates deflection towards channel B. 6.20 µm particles deflected towards channel B and 10 µm particles deflected into channel A. (For interpretation of the references to color in the figure caption, the reader is referred to the web version of the article.)

two different electric fields of 6.85 and 17.1 V/cm. Fig. 6(a) shows the particle fractions at two different electric fields, 6.85 V/cm (closed symbols) and 17.1 V/cm (open symbols) for channels 1 and 4 as function of conductivity. Higher particle fractions are seen in channel 4 at higher electric field compared to lower fields. At higher electric field (17.1 V/cm) and medium conductivities <6 mS/cm, better channel sorting was observed. At low conductivities, 6.85 V/cm (closed symbols) fields yielded more particle events in channel 4 while this trend is opposite at the higher conductivities. For 17.1 V/cm (open symbols) fields, the lower conductivities showed the same trend, but the trend reversal was not apparent at higher buffer conductivities.

Sorting efficiencies could likely be improved by manipulating the electric field strength since 17.1 V/cm DC fields provide higher sorting efficiencies compared to 6.85 V/cm. From Eq. (6), electric field strength increases the dielectrophoretic force experienced by the particle, which likely overcomes competing electrostatic particle interactions and nonlinear hydrodynamic effects in order to yield more efficient sorting. These electric field dependencies are roughly consistent between our lower voltage experimental results and simulations (see Figs. 3–5) and much can be learned from this operating regime. Simply operating at higher fields is not a solution because higher currents are not ideal for portable, battery operated sorting microdevices and produce adverse conditions for any biological samples.

### 4.4. Medium conductivity dependency ($\sigma_m$)

Dielectrophoretic force depends on medium conductivity properties as seen in the Clausius–Mossotti factor in Eqs. (6) and (7). Comparison of conductivity dependence was considered by examining the experimentally determined total particle fractions for all three particle sizes at 17.1 V/cm. Channel fraction variability was calculated by standard deviation (SD) using,

$$SD = \sqrt{\frac{1}{3}\sum_{Ch=1}^{4}\left(F^{Ch} - F_{avg}\right)^{2}} \tag{16}$$

Larger values of SD indicate better channel separations (Fig. 6(b)). From Fig. 6(b), greater SD values were found at 6 mS/cm or less, which indicates optimal buffer conditions to maximize DEP force based particle-bias in the device and thus more pronounced separations into channels. For most medium conductivities, 10 µm particles have better channel sorting efficiency. This conclusion is consistent with theoretical work showing that smaller particles experience DEP forces that are nearly the same order of magnitude as Brownian motion, gravity, and hydrodynamic effects; the DEP force dominates for larger particles [42].

Results from experiments show that medium conductivity also influences separation and sorting of particles to a degree similar to size differences and electric field. This parameter is overlooked in many DEP experiments. Also from experiments, the optimal buffer condition for maximizing spatial sorting into different channels of these three sized particles was 5.58 mS/cm.

### 4.5. Mapping into a 2-channel system

Experimental results for 6.20 µm and 10 µm particles in the 4-channel system were mapped into a 2-channel system to facilitate comparison with results from other groups of researchers [6]. The conditions and design considered are different [6] because they adopt: (1) 2-channel system, (2) different inlet position, (3) DC potential applied in a two inlet and two outlet ports configuration, and (4) electric fields 10–15 times greater than the applied electric field in this paper. Using Eqs. (17) and (18) to combine channels 1 and 2 into channel A and channels 3 and 4 into B is demonstrated in Fig. 6(c), The purpose of this exercise is to show the novelty in using lower electric fields and conductivities to achieve sorting of different sized particles. Particle fractions in the mapped two-channel system were calculated by:

$$F_A^c = F_1^c + F_2^c \tag{17}$$

$$F_B^c = F_3^c + F_4^c \tag{18}$$

Particle fraction difference $\delta$ between channels A and B was calculated as,

$$\delta = F_A^c + F_B^c \tag{19}$$

The deflection pattern for 6.20 μm particles is strongly towards channel B, but for 10 μm particles they were repelled from insulating obstacle region towards channel A. These results reproduce that of prior researchers [6] and supports observations that smaller particles experience smaller nDEP while larger particles experience greater nDEP forces away from the obstacle. Further examination of the dependence on medium conductivity shows greater average deflection of 6.20 μm particles with decreasing conductivities due to smaller nDEP force experienced by the particles. The 10 μm particles experience greater negative DEP force at the obstacle, thus displaying a more pronounced separation with decreasing conductivity. In all cases, streaming DEP is observed although the simulations suggest the conditions are close to those which would yield trapping DEP.

## 5. Conclusions

Direct current insulator-based dielectrophoresis (DC-iDEP) is a relatively new technique that emerged within the last decade. In this research, fluorescent polystyrene microparticle motion of three different sizes was studied in a PDMS microchannel with a rectangular insulating obstacle and four outlet channels by applying only DC electric fields at various buffer conductivities (0.50–8.50 mS/cm). The impact of the spatial field non-uniformities in the channel was studied by examining particle trajectories into four outlet channels. Particle deflection in DC-iDEP depends primarily on two forces: negative dielectrophoresis and electro-osmotic flow, although contributing nonlinear effects were attributed to particle/particle and particle/wall electrostatic interactions as well as to hydrodynamic fluid effects.

Particle size, DC electric field strength, and medium conductivity dependencies were studied in order to systematically discern the dielectrophoretic forces experienced by the particle under all these conditions. Electro-osmotic mobility did not vary considerably with different buffer conductivities. Simulations were carried out to compare the experimental work using *COMSOL Multiphysics*® software. From size dependency experiments and simulation results at 17.1 V/cm, 3.18 μm particles exhibited no channel preference, 6.20 μm particles experienced a weaker DEP force at the rectangular insulating obstacle, thus pushing particles into channel 4, while 10 μm particles experienced strongest negative DEP force repelling the particles into channels 1 and 2. Electric field dependency was studied employing two different electric field strengths (6.85 and 17.1 V/cm) with 6.20 μm particles; experimental and simulation results suggested that 17.1 V/cm yielded slightly better spatial sorting efficiencies compared to 6.85 V/cm. Medium conductivity dependency experiments revealed that lower conductivities achieve greater sorting efficiencies. The novelty of the research here is due to: (1) multiple outlet sorting with fine-tuning of DC electric field and medium conductivity, (2) lower DC electric fields achieved sorting and minimizes Joule heating effects, (3) device portability is realizable due to low DC voltages, and (4) particle sorting at low medium conductivities avoids electrolysis and minimizes electrode fouling.

The study presented here demonstrates multiparticle sorting at sufficiently low DC fields to avoid bio-particle damage thus illustrating the great potential of DC-iDEP to be employed for bacterial, protein, DNA, bacterial and mammalian cell manipulations with potential applications in medicine, food safety, biology and analytical chemistry. The properties of the medium (conductivity and pH), wall zeta potentials, and applied electric field could be further optimized to achieve higher efficiency sorting. DC-iDEP has great potential for use in portable diagnostic devices for easy, accurate and rapid analysis, and would be better adapted to diagnostic applications requiring larger cell event numbers. DC-iDEP technique is a viable option for disposable, inexpensive DEP microdevices since insulating-based-devices can be made from inexpensive substrates with simpler and more economical processes than embedded electrode-based-devices. Lastly, dielectrophoresis is a key technique to explore in these point-of-care devices due to operational simplicity, requirements of lower voltages, and small sample volumes, all of which enable device portability.

## Acknowledgements

Authors would like to thank the financial support provided by NSF CAREER 0644538 and special computer lab support provided by BioMEMS Research Chair (CAT 142) at Technologico de Monterrey.

## References

[1] A.R. Minerick, in: D. Li (Ed.), Encyclopedia of Micro- & Nanofluidics, Springer, Berlin, Heidelberg, New York, 2008.
[2] S.S. Keshavamurthy, K.M. Leonard, S.C. Burgess, A.R. Minerick, NSTI-Nanotech, Taylor & Francis, Boston, MA, 2008, p. 401.
[3] A.R. Minerick, AIChE J. 54 (2008) 2230.
[4] S.K. Srivastava, P.R. Daggolu, S. Burgess, A.R. Minerick, Electrophoresis 29 (2008) 5033.
[5] S. Srivastava, A. Gencoglu, A. Minerick, Anal. Bioanal. Chem. 399 (2011) 301.
[6] K.H. Kang, Y. Kang, X. Xuan, D. Li, Electrophoresis 27 (2006) 694.
[7] E.B. Cummings, A.K. Singh, Anal. Chem. 75 (2003) 4724.
[8] S. Ozuna-Chacón, B.H. Lapizco-Encinas, M. Rito-Palomares, S.O. Martínez-Chapa, C. Reyes-Betanzo, Electrophoresis 29 (2008) 3115.
[9] I. Barbulovic-Nad, X. Xuan, J.S.H. Lee, D. Li, Lab Chip 6 (2006) 274.
[10] P.K. Thwar, J.J. Linderman, M.A. Burns, Electrophoresis 28 (2007) 4572.
[11] Y. Kang, D. Li, S.A. Kalams, J.E. Eid, Biomed. Microdev. 10 (2008) 243.
[12] L. Zhang, F. Tatar, P. Turmezei, J. Bastemeijer, J.R. Mollinger, O. Piciu, A. Bossche, J. Phys. 34 (2006) 527.
[13] K.P. Chen, J.R. Pacheco, M.A. Hayes, S.J.R. Staton, Electrophoresis 30 (2009) 1441.
[14] M.D. Pysher, M.A. Hayes, Anal. Chem. 79 (2007) 4552.
[15] J. Zhu, T.-R.J. Tzeng, G. Hu, X. Xuan, Microfluid Nanofluid 7 (2009) 751.
[16] L. Zhang, J. Bastemeijer, J. Mollinger, A. Bossche, Proceedings of the 3rd IEEE International Conference on Nano/Micro Engineered and Molecular Systems, IEEE, Sanya, China, 2008, p. 864.
[17] B.H. Lapizco-Encinas, B.A. Simmons, E.B. Cummings, Y. Fintschenko, 7th International Conference on Miniaturized Chemical and Biochemical Analysis Systems, CA, USA, 2003, p. 607.
[18] B.H. Lapizco-Encinas, B.A. Simmons, E.B. Cummings, Y. Fintschenko, Electrophoresis 25 (2004) 1695.
[19] C.-P. Jen, Y.-H. Huang, T.-W. Chen, DTIP of MEMS & MOEMS, EDA Publishing, France, 2008.
[20] C.-P. Jen, T.-W. Chen, Microsyst. Technol. 15 (2009) 1141.
[21] B.G. Hawkins, A.E. Smith, Y.A. Syed, B.J. Kirby, Anal. Chem. 79 (2007) 7291.
[22] J. Zhu, X. Xuan, Electrophoresis 30 (2009) 2668.
[23] N. Lewpiriyawong, C. Yang, Y.C. Lam, Biomicrofluidics 2 (2008).
[24] Y.-K. Cho, S. Kim, K. Lee, C. Park, J.-G. Lee, C. Ko, Electrophoresis 30 (2009) 3153.
[25] R. Pethig, G.H. Markx, Trends Biotechnol. 15 (1997) 426.
[26] I. Ermolina, H. Morgan, J. Colloid Interface Sci. 285 (2005) 419.
[27] B.H. Lapizco-Encinas, B.A. Simmons, E.B. Cummings, Y. Fintschenko, Anal. Chem. 76 (2004) 1571.
[28] J.L. Baylon-Cardiel, B.H. Lapizco-Encinas, C. Reyes-Betanzo, A.V. Chavez-Santoscoy, S.O. Martinez-Chapa, Lab Chip 9 (2009) 2896.

[29] D.C. Duffy, J.C. McDonald, O.J.A. Schueller, G.M. Whitesides, Anal. Chem. 70 (1998) 4974.
[30] S. Bhattacharya, A. Datta, J.M. Berg, S. Gangopadhyay, J. Microelectromech. S14 (2005) 590.
[31] S.M. Hong, S.H. Kim, J.H. Kim, H.I. Hwang, J. Phys. 34 (2006) 656.
[32] X. Huang, M.J. Gordon, R.N. Zare, Anal. Chem. 60 (1988) 1837.
[33] Y. Berdichevsky, J. Khandurina, A. Guttman, Y.-H. Lo, Sens. Actuators B Chem. 97 (2004) 402.
[34] R.T. Kelly, T. Pan, A.T. Woolley, Anal. Chem. 77 (2005) 3536.
[35] J. Liu, T. Pan, A.T. Woolley, M.L. Lee, Anal. Chem. 76 (2004) 6948.
[36] X. Ren, M. Bachman, C. Sims, G.P. Li, N. Allbritton, J. Chromatogr. B 762 (2001) 117.
[37] Y.-H. Dou, N. Bao, J.-J. Xu, F. Meng, H.-Y. Chen, Electrophoresis 25 (2004) 3024.
[38] Y.-H. Dou, N. Bao, J.-J. Xu, H.-Y. Chen, Electrophoresis 23 (2002) 3558.
[39] W.K.T. Coltro, S.M. Lunte, E. Carrilho, Electrophoresis 29 (2008) 4928.
[40] D. Ross, T.J. Johnson, L.E. Locascio, Anal. Chem. 73 (2001) 2509.
[41] A.-J. Wang, J.-J. Xu, H.-Y. Chen, Anal. Chim. Acta 569 (2006) 188.
[42] N.G. Green, H. Morgan, J. Phys. 30 (1997) L41.